

Magnetoexcitons in phosphorene monolayers, bilayers, and van der Waals heterostructures

Roman Ya. Kezerashvili^{1,2} and Anastasia Spiridonova^{1,2}

¹*New York City College of Technology, The City University of New York, Brooklyn, NY 11201, USA*

²*The Graduate School and University Center, The City University of New York, New York, NY 10016, USA*

(Dated: August 22, 2021)

We study direct and indirect excitons in Rydberg states in phosphorene monolayers, bilayer and van der Waals (vdW) heterostructure in an external magnetic field, applied perpendicular to the monolayer or heterostructure within the framework of the effective mass approximation. Binding energies of magnetoexcitons are calculated by a numerical integration of the Schrödinger equation using the Rytova-Keldysh potential for direct magnetoexcitons and both the Rytova-Keldysh and Coulomb potentials for indirect one. The latter allows to understand the role of screening in phosphorene. We report the magnetic field energy contribution to the binding energies and diamagnetic coefficients (DMCs) for magnetoexcitons that strongly depend on the effective mass of electron and hole and their anisotropy and can be tuned by the external magnetic field. We demonstrate theoretically that the vdW phosphorene heterostructure is a novel category of 2D semiconductor offering a tunability of the binding energies of magnetoexcitons by mean of external magnetic field and control the binding energies and DMCs by the number of hBN layers separated two phosphorene sheets. Such tunability is potentially useful for the devices design.

I. INTRODUCTION

The most recent addition to the growing family of 2D material is phosphorene that is the monolayer of black phosphorus (BP). The BP is composed of individual phosphorene layers. The blossoming interest in phosphorene derives partially from its direct gap that is retained in both monolayer and bulk structure, high mobility, and high on-off current ratio in field-effective transistors [1–4]. In contrast, these characteristics simultaneously are not present in graphine, transitional metal dichalcogenides (TMDCs): WSe₂, WS₂, MoSe₂, MoS₂, or Xenos: silicene, germanene, stanene, making phosphorene a promising material for electronic and optical applications. Black phosphorus is the most stable of phosphorus allotropes. It was first synthesized in 1914 by Bridgman [5]. While bulk black phosphorus has interesting properties and was extensively studied in twentieth century [6–11], it was not used in the design of electronic devices.

However, everything has changed after the discovery of graphene in 2004 [12] which paved the way for two-dimensional materials. Initially, the research was focused on graphene [13, 14] and TMDCs [15–23] then silicene and other group VI elements have followed [24–27]. There are some drawbacks in the above materials. Graphene has high mobility and on-off ratio but a lack of a gap impedes its use in the design of electronic devices [2, 4]. TMDCs have a gap [28–30], but its carrier mobility is orders of magnitudes lower than in graphene. The phosphorene that has been synthesized in 2014 has advantages over graphene, TMDCs, and Xenos. Its most remarkable properties include thickness-dependent band gap, strong in-plane anisotropy, and high carrier mobility.

BP has a structure where monolayer appears to be composed of two distinct planes made of puckered honeycomb structure [31–33]. This results in an anisotropic electronic structure. Due to phosphorene unique topological structure and differences between the armchair (AC) and zigzag (ZZ) directions, it displays strong in-plane anisotropy. Many properties of phosphorene in these two principal directions are drastically different. The anisotropic structure is strongly reflected in effective masses of charge carriers and leads to anisotropic effective masses of electrons and holes along AC and ZZ (x and y) directions. Along the AC direction the effective electron and hole masses are smaller than along the ZZ direction [9, 31–33]. The distinct features of BP is that the direct gap located at the Γ point is preserved in the monolayer and bulk structure. This material is a direct band gap semiconductor with a strongly anisotropic dispersion in the vicinity of the gap. It is worth noting that the unusual structure of phosphorene sets it aside from graphene and other widely studied 2D semiconductors.

Since the synthesis of phosphorene, it has been extensively studied. For example, optical and thermal properties have been considered in Refs.[33–37], in plane electric field has been studied in Refs. [38–41], the effects of the strain on different properties of phosphorene have been addressed in Refs. [42–44], the Landau levels have been reported in Refs. [45–50].

Phosphorene hosts tightly bound excitons [31, 51–54]. Similarly to other monolayer semiconductors, reduced dimensionality and reduced screening of the Coulomb attraction lead to a high exciton binding energy in phosphorene. Moreover, the exciton binding energy in phosphorene is larger than the one in other 2D materials. Excitons in semiconductors in the presence of the external magnetic field have been studied for the past sixty years. Elliot and Loudon [55] and Hasegawa and Howard [56] developed the theory of the Mott exciton in the strong magnetic field.

Authors in Refs. [57–59] addressed Mott excitons. Excitons in TMDCs monolayers, bilayer, and the double-layer heterostructure in the presence of the external magnetic field have been extensively studied. The diamagnetic shifts have been reported in Refs. [23, 60–67], and Zeeman shifts have been reported in Refs [68–73]. We cite these works, but the recent literature on the subject is not limited by them. However, there is a lack of similar research on excitons in phosphorene. This motivates us to study the effect of the external magnetic field on the binding energies of Rydberg states of magnetoexcitons in monolayer, bilayer, and the double-layer heterostructure composed of phosphorene and to calculate diamagnetic coefficients (DMCs).

In this paper, we study the dependence of the magnetoexciton binding energy of Rydberg states: $1s$, $2s$, $3s$, and $4s$, on the external magnetic field perpendicular to a monolayer or heterostructure that is varied between 0 and 60 T and report the diamagnetic coefficients (i) for the direct magnetoexcitons in a freestanding (FS) and encapsulated phosphorene monolayers, (ii) for the indirect magnetoexciton in bilayer composed of two phosphorene monolayers, (iii) for the indirect magnetoexcitons in heterostructure formed by two phosphorene monolayers and separated by N hBN monolayers. The latter van der Waals heterostructure is denoted as vdW. In our approach, we numerically solve the Schrödinger equation for the magnetoexciton and obtain eigenfunctions and eigenvalues. Then we obtain the energy contribution from the magnetic field to the binding energies and use it to calculate diamagnetic coefficients. For the direct exciton, we solve the Schrödinger equation with the Rytova-Keldysh potential [74, 75], and for the indirect exciton, we solve the Schrödinger equation with the Rytova-Keldysh and the Coulomb potentials to understand the role of the screening in phosphorene.

The remainder of this paper is organized in the following way. In section II the theoretical model for the description of an electron-hole system in the external magnetic field with the charge carriers effective mass anisotropy is presented. Results of calculations of binding energies of Rydberg states and DMCs for direct magnetoexcitons in a freestanding and encapsulated phosphorene and indirect magnetoexcitons in FS bilayer and vdW phosphorene heterostructures are presented in Sec. III. Finally, conclusions follow in Sec. IV.

II. THEORETICAL MODEL

It is known that electrostatically-bound electrons and holes in the external magnetic field form magnetoexcitons. In this section, following Refs. [23, 27, 58, 67], we introduce briefly the theoretical model for the description of the Mott-Wannier magnetoexciton in phosphorene. We consider the energy contribution from the external magnetic field to the Rydberg states binding energies of magnetoexcitons and diamagnetic coefficients (DMCs). In the system under consideration, excitons are confined in a 2D freestanding and encapsulated phosphorene monolayer, FS bilayer phosphorene and van der Waals heterostructure, where N layers of hBN monolayers separate two phosphorene monolayers. In the latter two cases equal number of electrons and holes are located in parallel phosphorene monolayers at a distance D away. The corresponding schematic illustrations of these systems are shown in Fig. 1.

It is worth mentioning that we are considering the monolayers of hBN as an insulator. Phosphorene encapsulated between hBN layers is robust to oxidation and exhibits high mobilities. Moreover, hBN also has a high dielectric constant, resulting in a strong damping of the electrostatic repulsion by charged impurities which are responsible for the decrease of carriers mobility.

Let us introduce the coordinate vectors of the electron and hole for the Mott-Wannier exciton in the phosphorene layer. The following in-plane coordinates $\mathbf{r}_1 = (x_1, y_1)$ and $\mathbf{r}_2 = (x_2, y_2)$ for an electron and hole, respectively, will be used in our description. We assume that at low momentum $\mathbf{p} = (p_x, p_y)$, i.e., near the Γ point, the single electron and hole energy spectrum $\varepsilon_l^{(0)}(\mathbf{p})$ is given by

$$\varepsilon_l^{(0)}(\mathbf{p}) = \frac{p_x^2}{2m_x^l} + \frac{p_y^2}{2m_y^l}, \quad l = e, h, \quad (1)$$

where m_x^l and m_y^l are the electron and hole effective masses along the x and y directions, respectively. We assume that OX and OY axes correspond to the armchair and zigzag directions in a phosphorene monolayer, respectively.

The anisotropic nature of the 2D phosphorene atomic semiconductor, in contrary to other 2D isotropic materials such as graphene and TMDC semiconductors, breaks the central symmetry and requires for the description of excitons the use of the Cartesian coordinates. The asymmetry of the electron and hole dispersion in phosphorene is reflected in the Hamiltonian for the Mott-Wannier magnetoexciton, and within the framework of the effective mass approximation

the Hamiltonian for an interacting electron-hole pair in phosphorene in the external magnetic field reads ($\hbar = c = 1$)

$$\hat{H} = \frac{1}{2m_e^x} \left(i\nabla_{x_e} - eA_x(r_e) \right)^2 + \frac{1}{2m_e^y} \left(i\nabla_{y_e} - eA_y(r_e) \right)^2 + \frac{1}{2m_h^x} \left(i\nabla_{x_h} + eA_x(r_h) \right)^2 + \frac{1}{2m_h^y} \left(i\nabla_{y_h} + eA_y(r_h) \right)^2 + V(|\mathbf{r}_e - \mathbf{r}_h|), \quad (2)$$

where the m_i^j , $j = x, y$, $i = e, h$ correspond to the effective mass of the electron or hole in the x or y direction, respectively, and $V(|\mathbf{r}_e - \mathbf{r}_h|)$ describes the electrostatic interaction between the electron and hole. When the electron and hole are located in 2D plane, we use the Rytova-Keldysh (RK) potential [74, 75] that is widely used for the description of charge carriers interaction in 2D materials. The RK potential is a central potential, and the interaction between the electron and hole for direct excitons in a monolayer has the form [74, 75]:

$$V_{RK}(r) = -\frac{\pi k e^2}{2\kappa\rho_0} \left[H_0\left(\frac{r}{\rho_0}\right) - Y_0\left(\frac{r}{\rho_0}\right) \right], \quad (3)$$

where $r = r_e - r_h$ is the relative coordinate between the electron and hole. In Eq. (3), e is the charge of the electron, $\kappa = (\epsilon_1 + \epsilon_2)/2$ describes the surrounding dielectric environment, ϵ_1 and ϵ_2 are the dielectric constants below and above the monolayer, H_0 and Y_0 are the Struve and Bessel functions of the second kind, respectively, and ρ_0 is the screening length. The screening length ρ_0 can be written as $\rho_0 = 2\pi\chi_{2D}/\kappa$ [76], where χ_{2D} is the 2D polarizability, which in turn is given in [75]. At the long-range distances V_{RK} retains $1/r$ behavior as the Coulomb potential, for smaller distances the potential well is logarithmic.

Following the standard procedure [77] for the separation of the relative motion of the electron-hole pair from their center-of-mass motion one introduces variables for the center-of-mass of an electron-hole pair $\mathbf{R} = (X, Y)$ and the relative motion of an electron and a hole $\mathbf{r} = (x, y)$, as $X = (m_e^x x_1 + m_h^x x_2)/(m_e^x + m_h^x)$, $Y = (m_e^y y_1 + m_h^y y_2)/(m_e^y + m_h^y)$, $x = x_1 - x_2$, $y = y_1 - y_2$, $r^2 = x^2 + y^2$. The Schrödinger equation with Hamiltonian (2) has the form: $\hat{H}\Psi(\mathbf{r}_1, \mathbf{r}_2) = \mathcal{E}\Psi(\mathbf{r}_1, \mathbf{r}_2)$, where $\Psi(\mathbf{r}_1, \mathbf{r}_2)$ and \mathcal{E} are the eigenfunction and eigenenergy, respectively. One can write $\Psi(\mathbf{r}_1, \mathbf{r}_2)$ in the form $\Psi(\mathbf{r}_1, \mathbf{r}_2) = \Psi(\mathbf{R}, \mathbf{r}) = e^{i\mathbf{P}\cdot\mathbf{R}/\hbar}\Phi(x, y)$, where $\mathbf{P} = (P_x, P_y)$ is the momentum of the center-of-mass of the electron-hole pair and $\Phi(x, y)$ is the wave function of the relative motion of the electron-hole pair. Following Refs. [23, 27, 67, 78], after lengthy calculations one obtains the equation that describes the Mott–Wannier exciton in Rydberg optical states in the external magnetic field perpendicular to the phosphorene monolayer. Finally, the equation for

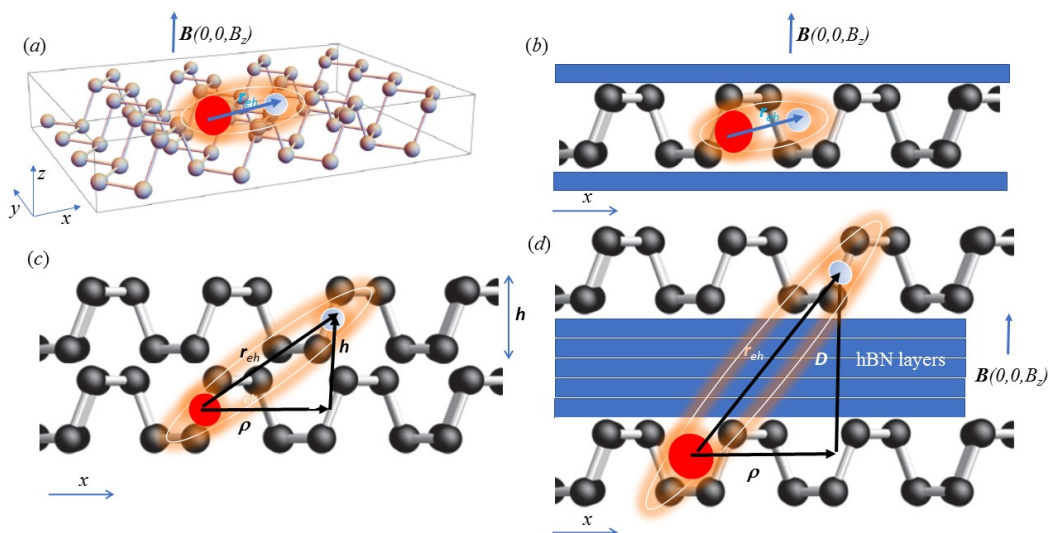


FIG. 1. (Color online) Schematic illustration of magnetoexcitons in phosphorene monolayers and heterostructures. (a) A direct magnetoexciton in a freestanding phosphorene monolayer. (b) A direct magnetoexciton in an encapsulated phosphorene monolayer. (c) An indirect magnetoexciton in a freestanding bilayer phosphorene heterostructure. (d) An indirect magnetoexciton in phosphorene van der Waals heterostructure.

the relative motion of the electron and hole in the phosphorene monolayer with zero center-of-mass momentum reads

$$\left[-\frac{1}{2\mu_x} \frac{\partial^2}{\partial x^2} - \frac{1}{2\mu_y} \frac{\partial^2}{\partial y^2} + \frac{e^2}{8\mu_x} B^2 x^2 + \frac{e^2}{8\mu_y} B^2 y^2 + V(x, y) \right] \Phi(x, y) = E\Phi(x, y). \quad (4)$$

where $\mu_x = \frac{m_x^e m_x^h}{m_x^e + m_x^h}$ and $\mu_y = \frac{m_y^e m_y^h}{m_y^e + m_y^h}$ are the reduced masses, related to the relative motion of an electron-hole pair in the x and y directions, respectively. In Eq. (4) the anisotropy is present in the kinetic and magnetic terms, while the potential term has isotropic form.

Following Refs. [79, 80] one can obtain from (4) the expectation value for the ground state energy. For the case of $V_{RK}(x, y)$ potential we have $E = \left\langle -\frac{1}{2\mu_x} \frac{\partial^2}{\partial x^2} \right\rangle + \left\langle -\frac{1}{2\mu_y} \frac{\partial^2}{\partial y^2} \right\rangle + \left\langle \frac{e^2}{8\mu_x} B^2 x^2 \right\rangle + \left\langle \frac{e^2}{8\mu_y} B^2 y^2 \right\rangle + \langle V_{RK}(x, y) \rangle$. The later expression could be viewed as the sum of the average values of the operators of kinetic and potential energies in 2D space obtained by using the corresponding eigenfunction $\Phi(x, y)$ of the exciton. Phosphorene exhibits charge carriers effective mass anisotropy with lighter effective masses along the armchair direction and heavier effective masses along the zigzag direction that leads to the reduced mass anisotropy: $\mu_y > \mu_x$. For the set of masses presented in Table I the ratio μ_y/μ_x varies from ~ 7 to 16. Therefore, from the latter expression one can conclude that contributions from the kinetic and magnetic energies to the total ground state energy can be by the order of magnitude different for AC and ZZ directions. In particular, the kinetic energy along the AC direction is much larger than that along the ZZ direction. Thus, the anisotropic nature of the 2D phosphorene atomic semiconductors, in contrast to other 2D materials such as graphene, Xenes, and TMDC semiconductors, allows excitons to be confined in a quasi-one-dimensional space predicted in theory [1, 81], leading to remarkable phenomena arising from the reduced dimensionality and screening. In Fig. 2 the total potential $W(x, y) = V_{RK}(x, y) + \frac{e^2}{8\mu_x} B^2 x^2 + \frac{e^2}{8\mu_y} B^2 y^2$ that acts on the electron-hole system in phosphorene is presented. One can observe the anisotropic structure of this potential and its asymmetry with respect to the AC and ZZ directions.

Let us now to consider the indirect magnetoexcitons formed by electrons and holes located in two different phosphorene monolayers in the bilayer or vdW heterostructure. In the latter case the phosphorene layers are separated by N layers of hBN monolayers. Such magnetoexcitons have a longer lifetime than the direct excitons due to longer recombination time. Equation (4) still describes the indirect exciton. However, for indirect excitons, the expressions for the interaction between the electron and hole in Eq. (4) can be written as:

$$V_{RK}(\sqrt{\rho^2 + D^2}) = -\frac{\pi k e^2}{2\kappa \rho_0} \left[H_0 \left(\frac{\sqrt{\rho^2 + D^2}}{\rho_0} \right) - Y_0 \left(\frac{\sqrt{\rho^2 + D^2}}{\rho_0} \right) \right], \quad (5)$$

for the RK potential, and

$$V_C(\sqrt{\rho^2 + D^2}) = -\frac{k e^2}{\kappa (\sqrt{\rho^2 + D^2})} \quad (6)$$

for the Coulomb potential and where $\rho^2 = x^2 + y^2$. Equations (5) and (6) describe the interaction between the electron and hole that are located in different parallel phosphorene monolayers separated by a distance $D = h + Nl_{\text{hBN}}$, where $l_{\text{hBN}} = 0.333$ nm is the thickness of the hBN layer and h is the phosphorene thickness given in Table I. Therefore, one can obtain the eigenfunctions and eigenenergies of magnetoexcitons by solving Eq. (4) using the potential (3) for direct magnetoexcitons, or using either potential (5) or (6) for indirect magnetoexcitons.

TABLE I. Parameters for phosphorene. Four sets of reduced masses for phosphorene that are used in calculations as input parameters. The anisotropic reduced masses μ_x and μ_y are obtained based on effective masses of the electron and hole given in Ref. [82] for the set 1, in Ref. [83] for the set 2, in Ref. [84] for the set 3, and in Ref.[1] for the set 4. μ_x and μ_y are in units of the electron mass, m_0 . χ_{2D} and h are the polarizability and thickness of phosphorene, respectively, in nm.

	μ_x	μ_y	μ_y/μ_x	χ_{2D} (nm)	h (nm)
set 1	0.06296	0.96774	15.37		
set 2	0.06667	0.88780	13.32	0.41 ^a	0.541 ^b
set 3	0.09122	0.6599	7.23		
set 4	0.07969	0.9498	11.92		

^a Reference [85].

^b Reference [86].

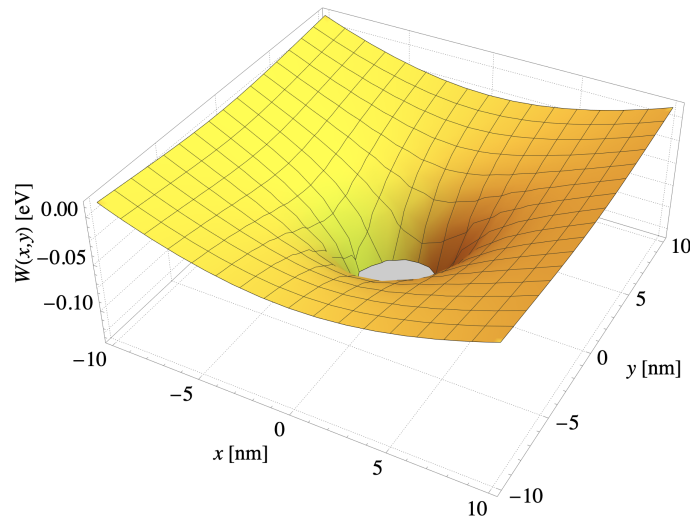


FIG. 2. Total potential $W(x, y) = V_{RK}(x, y) + \frac{e^2}{8\mu_x} B^2 x^2 + \frac{e^2}{8\mu_y} B^2 y^2$ is plotted as a function of x and y . $W(x, y)$ and x and y are given in eV and nm, respectively. The potential is calculated at $B = 30$ T with the parameters of the reduced masses of the set 1.

III. RESULTS OF CALCULATIONS AND DISCUSSION

We report the dependence of the energy contribution from the external magnetic field to the binding energies of magnetoexcitons in Rydberg states $1s$, $2s$, $3s$, and $4s$ in the FS (Fig. 1(a)) and encapsulated by hBN (Fig. 1(b)) phosphorene, the FS phosphorene bilayer (Fig. 1(c)), and the vdW heterostructure (Fig. 1(d)) on the magnetic field. The diamagnetic coefficients for the monolayers, bilayer, and vdW phosphorene heterostructure are reported for the first time.

In calculations, we use effective masses for electron and hole found in literature Refs. [1, 82–84], which are obtained by using the first principle calculations. The lattice constants in Refs. [1, 82–84] do not coincide with each other and different functionals for the correlation energy and setting parameters for the hopping lead to some difference in results for anisotropic masses. It is obvious that these can cause the difference in the band curvatures and, therefore, effective masses along the armchair and the zigzag directions. The latter motivate us to use in calculations of binding energies of magnetoexcitons and DMCs the different sets of masses from Refs. [1, 82–84] that allows to understand the dependence of the binding energy of magnetoexcitons and DMCs on effective masses of electrons and holes and the role of anisotropic masses. The corresponding reduced masses μ_x and μ_y along the armchair and zigzag directions, respectively, are given in Table I. We use these masses as input parameters and refer to them as the set 1, the set 2, the set 3, and the set 4. Below, we report results for the sets of masses 1 and 3 since they give an upper and lower bounds on the binding energies and the energy contribution from the magnetic field to the binding energies of the Rydberg states. Results from the sets of masses 2 and 4 fall within results of the sets 1 and 3.

A numerical solution of the Schrödinger equation (4), using the aforementioned interaction potentials and input parameters from Table I, is performed using the finite element method, which yields pairs of eigenenergies and eigenfunctions which are solutions to the Schrödinger equation, corresponding to the most-strongly-bound states. The method is based on using the finite element method implemented in Wolfram Mathematica in the NDEigensystem function. We modify the code successfully implemented in Ref. [36] in a way that it explicitly contains $\frac{e^2}{8\mu_x} B^2 x^2$ and $\frac{e^2}{8\mu_y} B^2 y^2$ terms. Our results for the binding energies of direct excitons in FS and encapsulated hBN phosphorene monolayers and indirect excitons in FS phosphorene bilayer for the masses sets 1 and 3 are given in Table II. One can see that the binding energy of excitons in FS and encapsulated monolayers significantly depend on the anisotropic reduced masses. Moreover, a much lower screening of excitons in the freestanding monolayer makes their binding energies, for example, in the ground state over three fold bigger than when the monolayer is encapsulated by hBN.

To check the validity of the code, we use the input parameters from respective papers listed below and calculate the binding energies of direct and indirect excitons. The code reproduces the theoretical binding energies of direct excitons in phosphorene and of indirect excitons in bilayer reported in Ref. [3], where binding energies are calculated using Wannier effective-mass theory in 2D space, within 8%. The binding energies for $1s$ state obtained using a semi-analytical perturbation theory approach [54] are reproduced within 4%. The code reproduces binding energies for $n = 0, \dots, 4$ states for FS phosphorene, phosphorene on SiO_2 substrate, and encapsulated by hBN phosphorene

TABLE II. Binding energies of direct magnetoexcitons in FS and encapsulated hBN phosphorene monolayers and indirect magnetoexcitons in FS phosphorene bilayer for the sets of masses 1 and 3. For indirect magnetoexcitons in the bilayer phosphorene binding energies are calculated using V_{RK} and V_C potentials. Energies are given in meV.

State	Monolayer				Bilayer			
	Set 1		Set 3		Set 1		Set 3	
	hBN	FS	hBN	FS	V_{RK}	V_C	V_{RK}	V_C
1s	187.94	718.71	199.66	746.06	388.88	827.17	395.54	854.03
2s	78.62	488.84	74.37	478.75	298.56	653.05	294.50	644.97
3s	53.83	394.04	50.35	377.72	248.52	525.71	239.53	501.07
4s	35.67	319.55	32.03	311.22	211.61	430.68	209.07	429.89

when energies obtained using numerical procedure where the Schrödinger equation is solved via a finite element representation of the exciton wave equation [87] within 1% and using $k \cdot p$ theory [88] within 4%.

A. Contribution from the external magnetic field to binding energies of magnetoexcitons in a monolayer

In Fig. 3 (a)-(b) we report the energy contribution from the external magnetic field to the binding energies of Rydberg states for direct magnetoexcitons in FS and encapsulated by hBN phosphorene, respectively, as a function of B^2 . We report results for the sets of masses 1 and 3. The dashed and solid boundary curves in Fig. 3 correspond to the results obtained with the sets of masses 1 and 3, respectively. The results from the sets of masses 2 and 4 fall in the shaded region.

Interestingly enough, in phosphorene, we observe the same tendencies for magnetoexcitons as in TMDCs [23, 67] and Xenex [27] monolayers. The binding energies and the energy contribution from the magnetic field to the binding energies of Rydberg states of magnetoexcitons strongly depend on the exciton reduced mass, even though phosphorene has anisotropic mass along x and y directions. The reduced mass of the exciton along the AC direction, depending on the set, is between seven and fifteen times smaller than the reduced mass along the ZZ direction. Since according to Eq. (4), the Schrödinger equation contains terms that are proportional to $\frac{1}{\mu_x}$ and $\frac{1}{\mu_y}$, the terms with significantly smaller μ_x dominate in Eq. (4). This is consistent with the anisotropic behavior of the potential $W(x, y)$ shown in Fig. 2 that exhibits the anisotropy with respect to the armchair and zigzag directions. Since the set 1 has the lowest μ_x and the highest μ_y , the set 3 is vice versa, we report results for the sets 1 and 3 as representative cases.

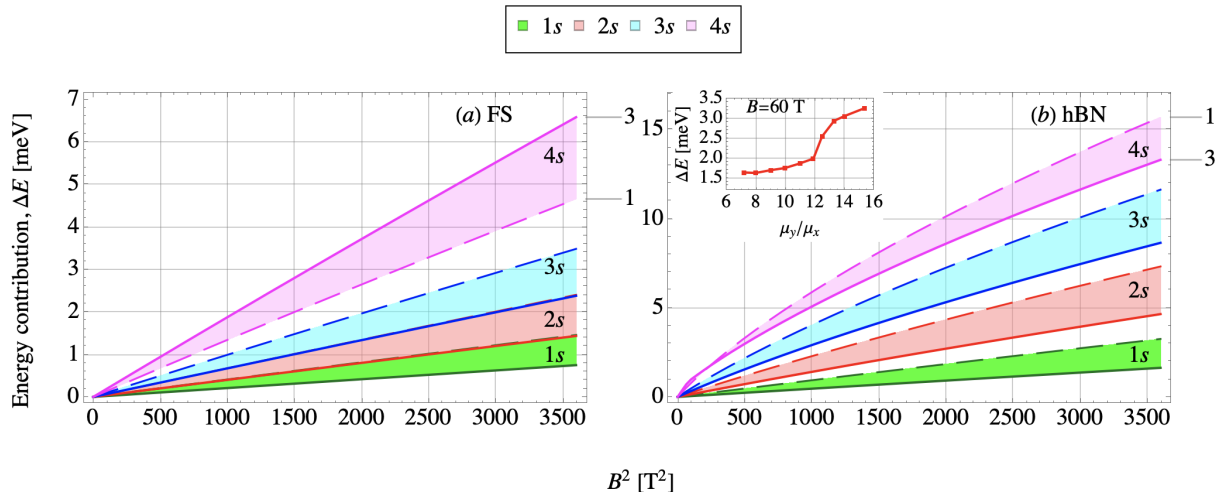


FIG. 3. Dependencies of the energy contribution from the magnetic field to the binding energies of magnetoexcitons in states 1s, 2s, 3s, and 4s for FS (a) and encapsulated by hBN (b) phosphorene monolayers on the squared magnetic field. The boundary dashed and solid curves correspond to the sets of masses 1 and set 3, respectively. The contributions for the sets of masses 2 and 4 fall within the shaded region. The inset in Fig. 3(b) shows the dependence of the energy contribution from the magnetic field on the ratio $\frac{\mu_y}{\mu_x}$.

Here should be noted that in contrast to binding energies of direct excitons in TMDCs and Xenex, the binding energies of direct excitons in phosphorene have more complicated dependence on the anisotropic reduced masses. In phosphorene the central symmetry is strongly broken due to the large anisotropy of the electron and hole effective masses. This can be observed, for example, in the encapsulated by hBN phosphorene. The insert in Fig. 3(b) shows the dependence of the magnetic field contribution to the binding energy of the direct magnetoexciton on the ratio $\frac{\mu_y}{\mu_x}$. Here we plot ΔE using the values $\frac{\mu_y}{\mu_x}$ from Table I. ΔE for $\frac{\mu_y}{\mu_x} = 8, 9, 10, 11, 12.5$ and 14 are calculated by extrapolation of μ_x from Refs. [1, 82–84] and obtaining corresponding μ_y using the value of $\frac{\mu_y}{\mu_x}$. The bigger $\frac{\mu_y}{\mu_x}$ ratio corresponds to the more anisotropic system that becomes quasi-one-dimensional [82], and the increase of $\frac{\mu_y}{\mu_x}$ leads to the increase of the contribution due to the magnetic field to the binding energy of the magnetoexciton. The character of these magnetoexcitons is that their spatial distribution of wave functions is strongly anisotropic. These magnetoexcitons form striped-like patterns, similar to those in nanotubes [89] or nanowires [90] that are 1D systems.

Interestingly, the set 1 with the lowest μ_x and the highest μ_y has the lowest $1s$ state binding energy, but for states $2s$, $3s$, and $4s$ the set 3 with the highest μ_x and the lowest μ_y gives the lowest binding energies. The binding energy percent difference between the sets 1 and 3 in states $2s$, $3s$, and $4s$ is 6%, 7%, and 11%, respectively. Also, based on Fig. 3(a), for states $1s$ - $3s$ the set 1 gives the highest energy contribution to the binding energy and the set 3 gives the lowest ΔE . However, for the state $4s$ the trend is reversed, and the set 3 gives the highest ΔE , and the set 1 gives the lowest ΔE . In addition, in contrast to magnetoexcitons that dissociate in the TMDCs and Xenex monolayers encapsulated by hBN [27], in states $3s$ and $4s$ the magnetoexcitons in phosphorene monolayers stay bound when the magnetic field is varied in the range from 0 to 60 T. This feature is also the result of quasi-1D character of magnetoexcitons in phosphorene.

B. Contribution from the external magnetic field to the binding energies of magnetoexcitons in bilayer and vdW heterostructure

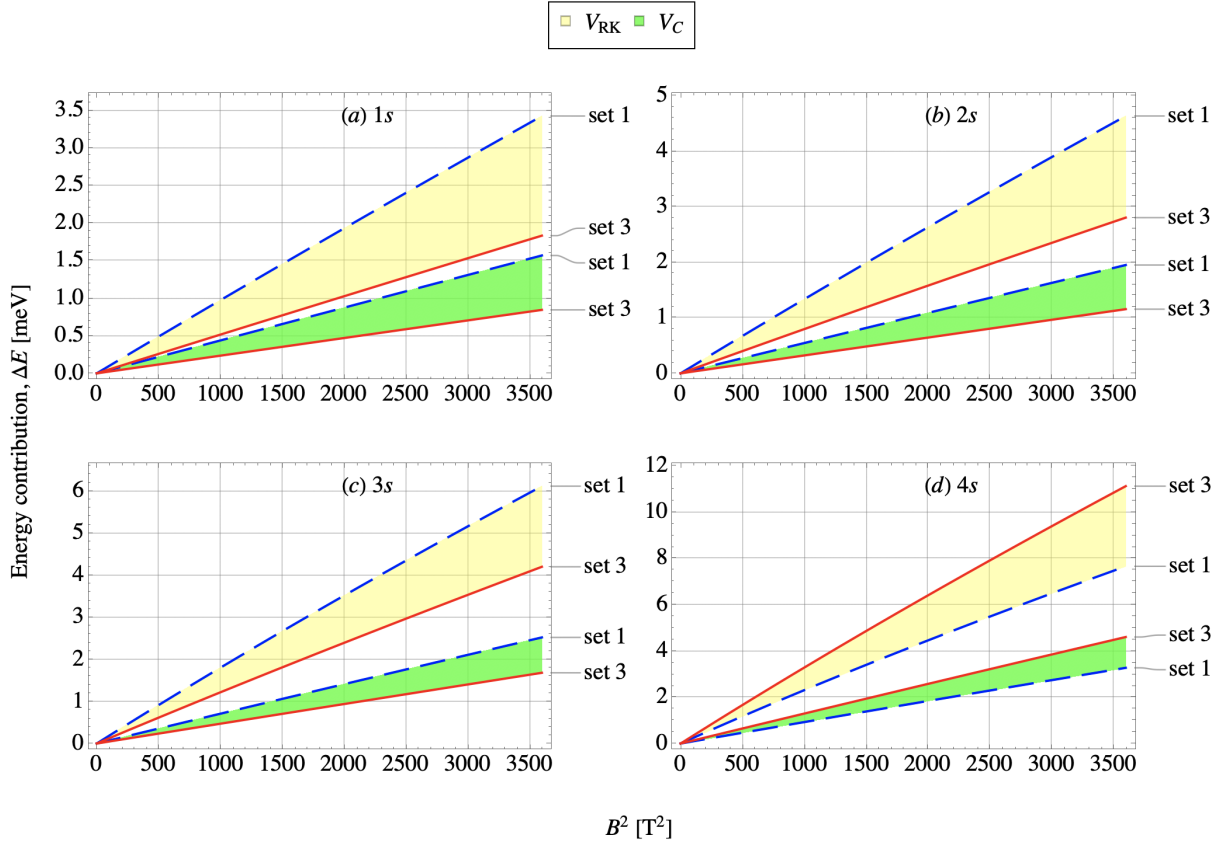


FIG. 4. The energy contribution from the magnetic field to the binding energy of Rydberg states $1s$ - $4s$ for the FS bilayer obtained using V_{RK} and V_C potentials. The boundary dashed and solid curves correspond to the sets of masses 1 and 3, respectively. The yellow and green shaded areas correspond to the calculations with V_{RK} and V_C potentials, respectively.

For indirect magnetoexcitons in the FS bilayer phosphorene and the vdW heterostructure, we examine how interaction potential affects Rydberg states binding energies and the energy contribution from the external magnetic field to the binding energies. In addition, for the vdW heterostructure, we consider an additional degree of freedom to tune binding energies by number of hBN layers that separate two phosphorene monolayer.

In Fig. 4, we report results for FS bilayer for the sets 1 and 3. The set 1 gives an upper bound on the energy contribution and is denoted by the dashed line. The set 3 gives a lower bound on ΔE and is denoted by the solid line. As was observed in the monolayer, in the state $4s$ in bilayer there is a flip of boundaries: the set 1 gives a lower boundary and the set 3 gives an upper boundary. Similar to results reported for magnetoexcitons in Xenes and TMDCs bilayer systems in Ref. [23, 27], in phosphorene bilayer, the following relation always holds $\Delta E_{RK} > \Delta E_C$. In addition, it is worth mentioning that energy contribution from the magnetic field to the binding energy is higher for indirect magnetoexcitons in the FS bilayer system than for direct magnetoexcitons in FS phosphorene. Based on the results in Table II for the bilayer phosphorene, Rydberg states binding energies calculated with the Coulomb potential are twice as big as the binding energies calculated with the Rytov-Keldysh potential. Similar to the monolayer system, magnetoexcitons in the bilayer in states $2s$, $3s$, and $4s$ are more bound than magnetoexcitons in TMDCs bilayer system.

For the vdW heterostructure, in Fig. 5 we compare ΔE_{RK} and ΔE_C . Results are given for the set 3 that is taken to be the representative case. We plot ΔE as a function of the external magnetic field and the number of hBN layers. As can be seen from Fig. 5 as the number of hBN layers increases ΔE_{RK} and ΔE_C converge.

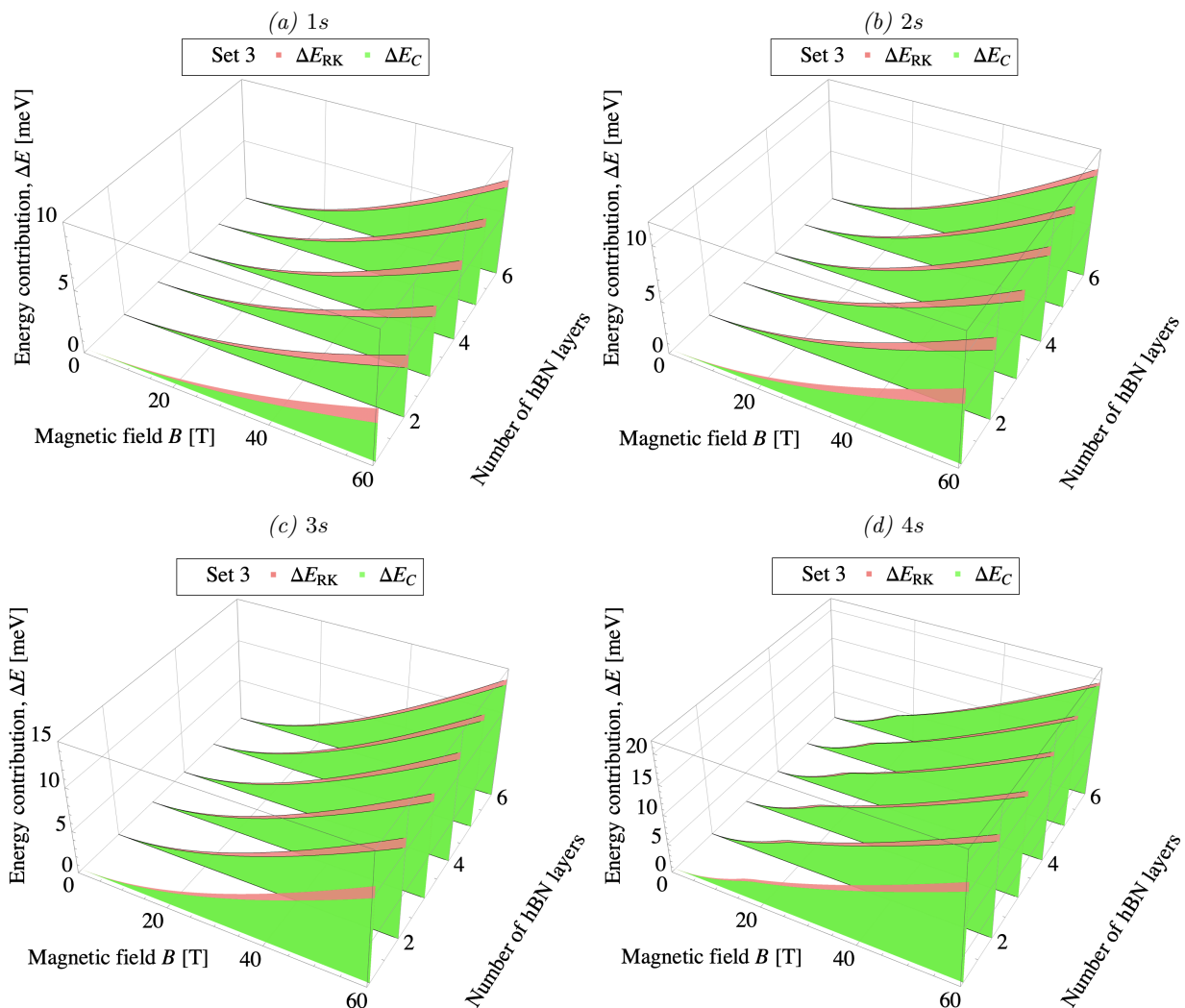


FIG. 5. The energy contribution for indirect magnetoexcitons in the vdW heterostructures as a function of the magnetic field and the number of hBN layers. The data are plotted for the set of masses 3.

TABLE III. Binding energies for indirect excitons in the van der Waals heterostructures calculated using V_{RK} and V_C potentials for the set of masses 3. Energies are given in meV.

N	V_{RK}				V_C			
	1s	2s	3s	4s	1s	2s	3s	4s
1	98.50	55.13	37.45	28.11	128.38	66.00	43.02	30.91
2	86.39	51.29	35.27	27.15	104.90	58.98	39.30	29.39
3	76.91	47.76	33.31	26.15	89.28	53.38	36.34	27.96
4	69.32	44.60	31.55	25.16	78.03	48.84	33.90	26.64
5	60.10	41.80	29.96	24.30	69.49	45.06	31.82	25.43
6	57.93	39.31	28.53	23.29	62.75	41.88	30.03	24.32

again, in contrast to indirect magnetoexcitons in TMDCs and Xenex double-layer heterostructure, magnetoexcitons in the vdW phosphorene heterostructure stay bound in states 3s and 4s while the magnetic field is varied between 0 and 60 T. This can be explained by the fact that the binding energies of states 3s and 4s are higher for indirect magnetoexcitons in phosphorene due to their effectively quasi-one-dimensional nature. The quasi-one-dimensionality of the magnetoexcitons in phosphorene is also demonstrated by the comparison of the contribution of the external magnetic field to binding energies of the vdW phosphorene heterostructure shown in Fig. 5 and TMDC heterostructures: ΔE due to the magnetic field in the vdW phosphorene heterostructure is always higher than the one in TMDC heterostructures. We report in Table III the binding energies of Rydberg states 1s, 2s, 3s, and 4s for $N=1,2,3,4,5,6$ when Eq. 4 is solved with V_{RK} and V_C . The binding energies calculated using the Coulomb potential are always larger than the one obtained with the RK potential. The increase of the phosphorene interlayer distance in the vdW heterostructure leads to the deduction of electron-hole interaction and results in the decrease of the binding energy of indirect magnetoexcitons.

IV. DIAMAGNETIC COEFFICIENTS

In this paper, we calculate the diamagnetic coefficients in the same fashion as was done in Refs. [23, 27, 67]. For phosphorene the diamagnetic coefficients for magnetoexcitons Rydberg states are reported for the first time. The magnetic field range between 0 and 30 T has been used to calculate the DMCs. In this range of the magnetic field one can observe the linear dependence of energy on B^2 . Here, we follow the notation in literature and denote the diamagnetic coefficient as σ . The diamagnetic coefficients for magnetoexcitons in monolayer and bilayer systems are reported in Table IV. σ for the indirect magnetoexcitons in the vdW heterostructure are reported in Table V.

TABLE IV. The diamagnetic coefficients, σ , of direct magnetoexcitons in FS and encapsulated by hBN monolayers for the sets of masses 1 and 3. σ is given in $\mu\text{eV}/\text{B}^2$. DMCs are obtained for the range of the magnetic field between 0 and 30 T and correspond to $R^2 = 0.9998$ for the linear regression model.

State	Monolayer				Bilayer			
	Set 1		Set 3		Set 1		Set 3	
	hBN	FS	hBN	FS	V_{RK}	V_C	V_{RK}	V_C
1s	0.94	0.41	0.46	0.21	0.97	0.44	0.52	0.23
2s	2.31	0.68	1.41	0.40	1.34	0.55	0.80	0.32
3s	4.13	0.99	2.96	0.67	1.81	0.71	1.22	0.47
4s		1.34		1.88	2.32	0.93	3.30	1.30

We report the diamagnetic coefficients in Table IV for two sets of masses. σ for the FS and encapsulated by hBN monolayers phosphorene is obtained when the magnetoexcitons interact through the V_{RK} interaction, while for the bilayer σ is given when Eq. (4) is solved using both V_{RK} and V_C potential. In the monolayer $\sigma_1 > \sigma_3$, where σ_1 and σ_3 are DMCs obtained with sets of masses 1 and 3, respectively. For phosphorene encapsulated by hBN, σ can be extracted in states 1s, 2s, and 3s. In the case of FS phosphorene σ can also be extracted in the state 4s. In the case of bilayer phosphorene, the diamagnetic coefficients can be extracted for 1s, 2s, 3s, and 4s states. This is different to the diamagnetic coefficients of bilayer composed of Xenex [27] and TMDCs [23], where σ cannot be extracted for all examined states.

TABLE V. The diamagnetic coefficients, σ , of indirect magnetoexcitons in the vdW heterostructure for the sets of masses 1 and 3. σ is given in $\mu\text{eV}/\text{B}^2$. DMCs are obtained for the range of the magnetic field between 0 and 30 T and correspond to $R^2 = 0.9998$ for the linear regression model.

State	N	Set 1		Set 3	
		V_{RK}	V_C	V_{RK}	V_C
1s	1	2.36	1.72	1.24	0.88
	2	2.80	2.22	1.49	1.16
	3	3.23	2.72	1.74	1.45
	4	3.67	3.20	2.00	1.73
	5	4.09	3.68	2.27	2.02
	6	4.51	4.14	2.53	2.30
2s	1	3.64	2.85	2.24	1.73
	2	4.04	3.37	2.50	2.06
	3	4.46	3.88	2.77	2.39
	4	4.88	4.38	3.05	2.71
	5			3.34	3.03
	6			3.62	3.35
3s	1				3.39

The DMCs for the vdW heterostructure are reported in Table V for two sets of masses when Eq. (4) is solved using V_{RK} and V_C potentials. σ can be extracted for the state 1s for all values of examined N , in the state 2s for the set 3 σ can be extracted for $N = 1, \dots, 6$. But for the set 1 in the state 2s, σ can be extracted only for $N = 1, \dots, 4$. From data listed in Tables IV and V, it follows that $\sigma_{RK} > \sigma_C$, where σ_{RK} and σ_C are the DMCs obtained using the RK and Coulomb potentials, respectively. Finally, our calculations show that the magnetoexcitons binding energies and DMCs in phosphorene vdW heterostructure can all be broadly tuned by changing the number of stacked hBN layers. This serves as a convenient and efficient method for engineering the materials properties.

V. CONCLUSIONS

In the framework of the excitonic Mott-Wannier model, we study direct and indirect excitons in Rydberg states in phosphorene monolayers, bilayer, and vdW heterostructure in the external magnetic field, applied perpendicular to the monolayer or heterostructure. We calculated the binding energies and DMCs for the Rydberg states 1s, 2s, 3s, and 4s for magnetoexcitons formed in these systems.

The magnetic field contribution to the binding energy of magnetoexcitons strongly depends on the effective masses of electron and hole and their anisotropy. Interestingly, the binding energies of magnetoexcitons are strongly correlated with the reduced mass anisotropy that makes magnetoexcitons in phosphorene effectively quasi-1D quasiparticles. An overall, the unique anisotropic character of these magnetoexcitons in phosphorene leads to the larger contribution to the binding energy than in TMDC materials.

The DMCs demonstrate the strong dependence on the effective electron-hole masses: DMCs in phosphorene monolayers, bilayer, and vdW heterostructure for the set 1 are about two fold bigger than the one for the set 2. The other distinct feature for the diamagnetic coefficients in the bilayer and vdW heterostructures is that σ calculated using the Coulomb potential is always smaller than DMCs obtained with the Rytova-Keldysh potential. In other word, the reduced dimensionality and screening increase the diamagnetic coefficients.

We show that the binding energy of direct and indirect magnetoexcitons can be tuned by the external magnetic field. Also, the binding energy of indirect excitons and DMC could be efficiently tuned by the stacking hBN layers. Such tunability of binding energies and DMCs is potentially useful for the devices design.

Finally, in summary, we have shown theoretically that the vdW phosphorene heterostructure is a novel category of 2D semiconductor offering a tunability of the binding energies of magnetoexcitons by mean of the external magnetic field and control by the number of hBN layers separating two phosphorene sheets. Also, the DMCs in the vdW heterostructure are tunable by controlling the number of hBN layers that separate two phosphorene layers. Thus, phosphorene provides a unique platform for novel optoelectronic applications and the exploration of the role of the symmetry breaking in anisotropic exciton physics.

Acknowledgments. This work is supported by the U.S. Department of Defense under Grant No. W911NF1810433

and PSC-CUNY Award No. 62261-00 50.

-
- [1] J. Qiao, X. Kong, Z.-X. Hu, F. Yang, and W. Ji, High-mobility transport anisotropy and linear dichroism in few-layer black phosphorus, *Nat. Commun.* **5**, 4475 (2014).
- [2] H. Liu, A. T. Neal, Z. Zhu, Z. Luo, X. Xu, D. Tománek, and P. D. Ye, Phosphorene: An unexplored 2D semiconductor with a high hole mobility, *ACS Nano* **8**, 4033 (2014).
- [3] A. Castellanos-Gomez, L. Vicarelli, E. Prada, J. O. Island, K. L. Narasimha-Acharya, S. I. Blanter, D. J. Groenendijk, M. Buscema, G. A. Steele, J. V. Alvarez, *et al.*, Isolation and characterization of few-layer black phosphorus, *2D Mater.* **1**, 025001 (2014).
- [4] L. Li, Y. Yu, G. J. Ye, Q. Ge, X. Ou, H. Wu, D. Feng, X. H. Chen, and Y. Zhang, Black phosphorus field-effect transistors, *Nat. Nanotechnol.* **9**, 372 (2014).
- [5] P. W. Bridgman, Two new modifications of phosphorus, *J. Am. Chem. Soc.* **36**, 1344 (1914).
- [6] R. W. Keyes, The electrical properties of black phosphorus, *Phys. Rev.* **92**, 580 (1953).
- [7] D. Warschauer, Electrical and optical properties of crystalline black phosphorus, *J. Appl. Phys.* **34**, 1853 (1963).
- [8] L. Cartz, S. R. Srinivasa, R. J. Riedner, J. D. Jorgensen, and T. G. Worlton, Effect of pressure on bonding in black phosphorus, *J. Chem. Phys.* **71**, 1718 (1979).
- [9] Y. Takao and A. Morita, Electronic structure of black phosphorus: Tight binding approach, *Physica B+C* **105**, 93 (1981).
- [10] A. Morita, Semiconducting black phosphorus, *Appl. Phys. A* **39**, 227 (1986).
- [11] B. Nöläng, O. Eriksson, and B. Johansson, The cohesive energy and band structure of black phosphorus, *J. Phys. Chem. Solids* **51**, 1025 (1990).
- [12] K. S. Novoselov, A. K. Geim, S. V. Morozov, D. Jiang, Y. Zhang, S. V. Dubonos, I. V. Grigorieva, and A. A. Firsov, Electric field effect in atomically thin carbon films, *Science* **306**, 666 (2004).
- [13] A. H. Castro Neto, F. Guinea, N. M. R. Peres, K. S. Novoselov, and A. K. Geim, The electronic properties of graphene, *Rev. Mod. Phys.* **81**, 109 (2009).
- [14] P. Avouris, T. F. Heinz, and T. Low, *2D materials: Properties and devices* (Cambridge University Press, 2017).
- [15] R. Cheng, D. Li, H. Zhou, C. Wang, A. Yin, S. Jiang, Y. Liu, Y. Chen, Y. Huang, and X. Duan, Electroluminescence and photocurrent generation from atomically sharp WSe₂/MoS₂ heterojunction p–n diodes, *Nano Lett.* **14**, 5590 (2014).
- [16] C.-H. Lee, G.-H. Lee, A. Zande, W. Chen, Y. Li, M. Han, X. Cui, G. Arefe, C. Nuckolls, T. Heinz, *et al.*, Atomically thin p–n junctions with van der Waals heterointerfaces, *Nat. Nanotechnol.* **9**, 676–681 (2014).
- [17] O. Cotlet, S. Zeytinoglu, M. Sigrist, E. Demler, and A. Imamoglu, Superconductivity and other collective phenomena in a hybrid Bose-Fermi mixture formed by a polariton condensate and an electron system in two dimensions, *Phys. Rev. B* **93**, 054510 (2016).
- [18] S. Manzeli, D. Ovchinnikov, D. Pasquier, O. V. Yazyev, and A. Kis, 2D transition metal dichalcogenides, *Nat. Rev. Mater.* **2**, 17033 (2017).
- [19] O. L. Berman and R. Ya. Kezerashvili, High-temperature superfluidity of the two-component Bose gas in a transition metal dichalcogenide bilayer, *Phys. Rev. B* **93**, 245410 (2016).
- [20] O. L. Berman and R. Ya. Kezerashvili, Superfluidity of dipolar excitons in a transition metal dichalcogenide double layer, *Phys. Rev. B* **96**, 094502 (2017).
- [21] G. Wang, A. Chernikov, M. M. Glazov, T. F. Heinz, X. Marie, T. Amand, and B. Urbaszek, Colloquium: Excitons in atomically thin transition metal dichalcogenides, *Rev. Mod. Phys.* **90**, 021001 (2018).
- [22] M. N. Brunetti, O. L. Berman, and R. Ya. Kezerashvili, Optical absorption by indirect excitons in a transition metal dichalcogenide/hexagonal boron nitride heterostructure, *J. Phys.: Condens. Matter* **30**, 225001 (2018).
- [23] R. Y. Kezerashvili and A. Spiridonova, Magnetoexcitons in transition metal dichalcogenides monolayers, bilayers, and van der Waals heterostructures, *Phys. Rev. Res.* **3**, 033078 (2021).
- [24] L. Matthes, O. Pulci, and F. Bechstedt, Massive dirac quasiparticles in the optical absorbance of graphene, silicene, germanene, and tinene, *J. Phys.: Condens. Matter* **25**, 395305 (2013).
- [25] A. Molle, J. Goldberger, M. Houssa, Y. Xu, S.-C. Zhang, and D. Akinwande, Buckled two-dimensional Xene sheets, *Nat. Mater.* **16**, 163 (2017).
- [26] J. Zheng, Y. Xiang, C. Li, R. Yuan, F. Chi, and Y. Guo, All-optically controlled topological transistor based on Xenos, *Phys. Rev. Applied* **14**, 034027 (2020).
- [27] R. Y. Kezerashvili and A. Spiridonova, Effects of parallel electric and magnetic fields on Rydberg excitons in buckled two-dimensional materials, *Phys. Rev. B* **103**, 165410 (2021).
- [28] K. F. Mak, C. Lee, J. Hone, J. Shan, and T. F. Heinz, Atomically thin MoS₂: A new direct-gap semiconductor, *Phys. Rev. Lett.* **105**, 136805 (2010).
- [29] A. Splendiani, L. Sun, Y. Zhang, T. Li, J. Kim, C.-Y. Chim, G. Galli, and F. Wang, Emerging photoluminescence in monolayer MoS₂, *Nano Lett.* **10**, 1271 (2010).
- [30] S. Tongay, J. Zhou, C. Ataca, K. Lo, T. S. Matthews, J. Li, J. C. Grossman, and J. Wu, Thermally driven crossover from indirect toward direct bandgap in 2D semiconductors: MoSe₂ versus MoS₂, *Nano Lett.* **12**, 5576 (2012).
- [31] A. Carvalho, M. Wang, X. Zhu, A. S. Rodin, H. Su, and A. H. Castro Neto, Phosphorene: from theory to applications, *Nat. Rev. Mater.* **1**, 16061 (2016).

- [32] M. Batmunkh, M. Bat-Erdene, and J. G. Shapter, Phosphorene and phosphorene-based materials – prospects for future applications, *Adv. Mater.* **28**, 8586 (2016).
- [33] D. Y. Qiu, F. H. da Jornada, and S. G. Louie, Environmental screening effects in 2D materials: Renormalization of the bandgap, electronic structure, and optical spectra of few-layer black phosphorus, *Nano Lett.* **17**, 4706 (2017).
- [34] T. Low, A. S. Rodin, A. Carvalho, Y. Jiang, H. Wang, F. Xia, and A. H. Castro Neto, Tunable optical properties of multilayer black phosphorus thin films, *Phys. Rev. B* **90**, 075434 (2014).
- [35] M. Ezawa, Topological origin of quasi-flat edge band in phosphorene, *New J. Phys.* **16**, 115004 (2014).
- [36] M. N. Brunetti, O. L. Berman, and R. Y. Kezerashvili, Optical properties of anisotropic excitons in phosphorene, *Phys. Rev. B* **100**, 155433 (2019).
- [37] S. Yoon, T. Kim, S.-Y. Seo, S.-H. Shin, S.-B. Song, B. J. Kim, K. Watanabe, T. Taniguchi, G.-H. Lee, M.-H. Jo, *et al.*, Electrical control of anisotropic and tightly bound excitons in bilayer phosphorene, *Phys. Rev. B* **103** (2021).
- [38] S. P. Koenig, R. A. Doganov, H. Schmidt, A. H. Castro Neto, and B. Özyilmaz, Electric field effect in ultrathin black phosphorus, *Appl. Phys. Lett.* **104**, 103106 (2014).
- [39] A. Chaves, T. Low, P. Avouris, D. Çakır, and F. M. Peeters, Anisotropic exciton stark shift in black phosphorus, *Phys. Rev. B* **91**, 155311 (2015).
- [40] P. Le and M. Yarmohammadi, Tuning thermoelectric transport in phosphorene through a perpendicular magnetic field, *Chem. Phys.* **519**, 1 (2019).
- [41] H. Kamban and T. Pedersen, Interlayer excitons in van der Waals heterostructures: Binding energy, Stark shift, and field-induced dissociation, *Sci. Rep.* **10** (2020).
- [42] A. S. Rodin, A. Carvalho, and A. H. Castro Neto, Strain-induced gap modification in black phosphorus, *Phys. Rev. Lett.* **112**, 176801 (2014).
- [43] Y. Li, S. Yang, and J. Li, Modulation of the electronic properties of ultrathin black phosphorus by strain and electrical field, *J. Phys. Chem. C* **118**, 23970 (2014).
- [44] H. Y. Lv, W. J. Lu, D. F. Shao, and Y. P. Sun, Enhanced thermoelectric performance of phosphorene by strain-induced band convergence, *Phys. Rev. B* **90**, 085433 (2014).
- [45] X. Zhou, W.-K. Lou, F. Zhai, and K. Chang, Anomalous magneto-optical response of black phosphorus thin films, *Phys. Rev. B* **92**, 165405 (2015).
- [46] X. Y. Zhou, R. Zhang, J. P. Sun, Y. L. Zou, D. Zhang, W. K. Lou, F. Cheng, G. H. Zhou, F. Zhai, and K. Chang, Landau levels and magneto-transport property of monolayer phosphorene, *Sci. Rep.* **5**, 12295 (2015).
- [47] M. Tahir, P. Vasilopoulos, and F. M. Peeters, Magneto-optical transport properties of monolayer phosphorene, *Phys. Rev. B* **92**, 045420 (2015).
- [48] P. E. Faria Junior, M. Kurpas, M. Gmitra, and J. Fabian, $k \cdot p$ theory for phosphorene: Effective g -factors, Landau levels, and excitons, *Phys. Rev. B* **100**, 115203 (2019).
- [49] J. Zhou, T.-Y. Cai, and S. Ju, Anisotropic exciton excitations and optical properties of hitorf's phosphorene, *Phys. Rev. Res.* **2**, 033288 (2020).
- [50] J.-Y. Wu, W.-P. Su, and G. Gumbs, Anomalous magneto-transport properties of bilayer phosphorene, *Sci. Rep.* **10**, 7674 (2020).
- [51] V. Tran, R. Fei, and L. Yang, Quasiparticle energies, excitons, and optical spectra of few-layer black phosphorus, *2D Mater.* **2**, 044014 (2015).
- [52] X. Wang, A. M. Jones, K. L. Seyler, V. Tran, Y. Jia, H. Zhao, H. Wang, L. Yang, X. Xu, and F. Xia, Highly anisotropic and robust excitons in monolayer black phosphorus, *Nat. Nanotechnol.* **10**, 517 (2015).
- [53] R. Tian, R. Fei, S. Hu, T. Li, B. Zheng, Y. Shi, J. Zhao, L. Zhang, X. Gan, and X. Wang, Observation of excitonic series in monolayer and few-layer black phosphorus, *Phys. Rev. B* **101**, 235407 (2020).
- [54] J. C. G. Henriques and N. M. R. Peres, Excitons in phosphorene: A semi-analytical perturbative approach, *Phys. Rev. B* **101**, 035406 (2020).
- [55] R. Elliott and R. Loudon, Theory of the absorption edge in semiconductors in a high magnetic field, *J. Phys. Chem. Solids* **15**, 196 (1960).
- [56] H. Hasegawa and R. Howard, Optical absorption spectrum of hydrogenic atoms in a strong magnetic field, *J. Phys. Chem. Solids* **21**, 179 (1961).
- [57] M. Shinada and S. Sugano, Optical absorption edge in layer-type semiconductors, *J. Phys. Soc. Jpn.* **20**, 1274 (1965).
- [58] L. P. Gor'kov and I. E. Dzialoshinskii, Contribution to the theory of the Mott exciton in a strong magnetic field, *Zh. Eksp. Teor. Fiz.* **53**, 717 (1967).
- [59] O. Akimoto and H. Hasegawa, Interband optical transitions in extremely anisotropic semiconductors. II. Coexistence of exciton and the Landau levels, *J. Phys. Soc. Jpn.* **22**, 181 (1967).
- [60] S. N. Walck and T. L. Reinecke, Exciton diamagnetic shift in semiconductor nanostructures, *Phys. Rev. B* **57**, 9088 (1998).
- [61] F. Luckert, M. Yakushev, C. Faugeras, A. Karotki, A. Mudryi, and R. Martin, Diamagnetic shift of the A free exciton in CuGaSe₂ single crystals, *Appl. Phys. Lett.* **97**, 162101 (2010).
- [62] B. Choi, Y. Kim, and J. Song, Diamagnetic shift of a InGaP-AlInGaP semiconductor single quantum well under pulsed-magnetic fields, *Appl. Sci. Converg. Technol* **24**, 156 (2015).
- [63] M. Van der Donck, M. Zarenia, and F. M. Peeters, Excitons, trions, and biexcitons in transition-metal dichalcogenides: Magnetic-field dependence, *Phys. Rev. B* **97**, 195408 (2018).
- [64] M. Van der Donck, M. Zarenia, and F. M. Peeters, Strong valley Zeeman effect of dark excitons in monolayer transition metal dichalcogenides in a tilted magnetic field, *Phys. Rev. B* **97**, 081109 (2018).

- [65] A. V. Stier, N. P. Wilson, K. A. Velizhanin, J. Kono, X. Xu, and S. A. Crooker, Magneto-optics of exciton Rydberg states in a monolayer semiconductor, *Phys. Rev. Lett.* **120**, 057405 (2018).
- [66] B. Han, C. Robert, E. Courtade, M. Manca, S. Shree, T. Amand, P. Renucci, T. Taniguchi, K. Watanabe, X. Marie, *et al.*, Exciton states in monolayer MoSe₂ and MoTe₂ probed by upconversion spectroscopy, *Phys. Rev. X* **8**, 031073 (2018).
- [67] A. Spiridonova, Magnetoexcitons in monolayer transition-metal dichalcogenides, *Phys. Lett. A* **384**, 126850 (2020).
- [68] Y. Li, J. Ludwig, T. Low, A. Chernikov, X. Cui, G. Arefe, Y. D. Kim, A. M. van der Zande, A. Rigosi, H. M. Hill, *et al.*, Valley splitting and polarization by the Zeeman effect in monolayer MoSe₂, *Phys. Rev. Lett.* **113**, 266804 (2014).
- [69] A. Srivastava, M. Sidler, A. Allain, D. Lembke, A. Kis, and A. Imamoglu, Valley Zeeman effect in elementary optical excitations of a monolayer WSe₂, *Nat. Phys.* **11** (2014).
- [70] G. Aivazian, Z. Gong, A. Jones, R.-L. Chu, J.-Q. Yan, D. Mandrus, C. Zhang, D. Cobden, W. Yao, and X. Xu, Magnetic control of valley pseudospin in monolayer WSe₂, *Nat. Phys.* **11**, 148 (2015).
- [71] D. MacNeill, C. Heikes, K. F. Mak, Z. Anderson, A. Kormányos, V. Zólyomi, J. Park, and D. C. Ralph, Breaking of valley degeneracy by magnetic field in monolayer MoSe₂, *Phys. Rev. Lett.* **114**, 037401 (2015).
- [72] G. Plechinger, P. Nagler, A. Arora, A. Aguila, M. Ballottin, T. Frank, P. Steinleitner, M. Gmitra, J. Fabian, P. Christianen, *et al.*, Excitonic valley effects in monolayer WS₂ under high magnetic fields, *Nano Lett.* **16** (2016).
- [73] A. Stier, K. McCreary, B. Jonker, J. Kono, and S. Crooker, Exciton diamagnetic shifts and valley Zeeman effects in monolayer WS₂ and MoS₂ to 65 Tesla, *Nat. Commun.* **7**, 10643 (2016).
- [74] N. Rytova, Screened potential of a point charge in a thin film, *Proc. Moscow State University, Phys. Astron.* **3**, 30 (1967).
- [75] L. V. Keldysh, Coulomb interaction in thin semiconductor and semimetal films, *JETP Lett* **29**, 658 (1979).
- [76] T. C. Berkelbach, M. S. Hybertsen, and D. R. Reichman, Theory of neutral and charged excitons in monolayer transition metal dichalcogenides, *Phys. Rev. B* **88**, 045318 (2013).
- [77] L. D. Landau and E. M. Lifshitz, *Quantum mechanics: non-relativistic theory*, third edition, revised and enlarged. ed. (Pergamon Press, Oxford, 1977).
- [78] A. H. MacDonald and D. S. Ritchie, Hydrogenic energy levels in two dimensions at arbitrary magnetic fields, *Phys. Rev. B* **33**, 8336 (1986).
- [79] R. Ya. Kezerashvili, Few-body systems in condensed matter physics, *Few-Body Syst.* **60**, 52 (2019).
- [80] R. Ya. Kezerashvili, *Recent Progress in Few-Body Physics*, edited by N. A. Orr, M. Płoszajczak, F. M. Marqués, and J. Carbonell (Springer International Publishing, Cham, 2020) pp. 827–831.
- [81] V. Tran, R. Soklaski, Y. Liang, and L. Yang, Layer-controlled band gap and anisotropic excitons in few-layer black phosphorus, *Phys. Rev. B* **89**, 235319 (2014).
- [82] X. Peng, Q. Wei, and A. Copple, Strain-engineered direct-indirect band gap transition and its mechanism in two-dimensional phosphorene, *Phys. Rev. B* **90**, 085402 (2014).
- [83] V. Tran and L. Yang, Scaling laws for the band gap and optical response of phosphorene nanoribbons, *Phys. Rev. B* **89**, 245407 (2014).
- [84] C. J. Páez, K. DeLello, D. Le, A. L. C. Pereira, and E. R. Mucciolo, Disorder effect on the anisotropic resistivity of phosphorene determined by a tight-binding model, *Phys. Rev. B* **94**, 165419 (2016).
- [85] A. S. Rodin, A. Carvalho, and A. H. Castro Neto, Excitons in anisotropic two-dimensional semiconducting crystals, *Phys. Rev. B* **90**, 075429 (2014).
- [86] P. Kumar, B. S. Bhadoria, S. Kumar, S. Bhowmick, Y. S. Chauhan, and A. Agarwal, Thickness and electric-field-dependent polarizability and dielectric constant in phosphorene, *Phys. Rev. B* **93**, 195428 (2016).
- [87] H. C. Kamban, T. G. Pedersen, and N. M. R. Peres, Anisotropic Stark shift, field-induced dissociation, and electroabsorption of excitons in phosphorene, *Phys. Rev. B* **102**, 115305 (2020).
- [88] P. E. Faria Junior, M. Kurpas, M. Gmitra, and J. Fabian, $k \cdot p$ theory for phosphorene: Effective g -factors, Landau levels, and excitons, *Phys. Rev. B* **100**, 115203 (2019).
- [89] I. V. Bondarev, Asymptotic exchange coupling of quasi-one-dimensional excitons in carbon nanotubes, *Phys. Rev. B* **83**, 153409 (2011).
- [90] R. Ya. Kezerashvili, Z. Machavariani, B. Beradze, and T. Tchelidze, Trions and biexcitons in ZnO/ZnMgO, CdSe/ZnS and CdSe/CdS core/shell nanowires, *Phys. E* **109**, 228 (2019).